processes

MDPI

Article

Natural Convection in a Circular Enclosure with Four Cylinders under Magnetic Field: Application to Heat Exchanger

Raouia Azzouz [1] and Mohamed Bechir Ben Hamida [1,2,3,*]

[1] Research Laboratory of Ionized Backgrounds and Reagents Studies (EMIR), Preparatory Institute for Engineering Studies of Monastir (IPEIM), University of Monastir, Monastir City 5000, Tunisia; raouia.azzouz@yahoo.com
[2] College of Engineering, Imam Mohammad Ibn Saud Islamic University (IMSIU), Riyadh 11423, Saudi Arabia
[3] Higher School of Sciences and Technology of Hammam Sousse (ESSTHS), University of Sousse, Sousse 4000, Tunisia
* Correspondence: mbhamida@imamu.edu.sa or benhamida_mbechir@yahoo.fr

Abstract: This paper documents the 2D numerical study of magnetohydrodynamic unsteady natural convective heat transfer in a circular enclosure with four heating cylinders in both the horizontal and the vertical mid-plane. The fluid is an incompressible Newtonian fluid. The main transport equations based on the conservation of mass, momentum, and energy are calculated and solved using a finite element numerical solver with the following parameter ranges: dimensionless distance between cylinders S = 0.05–0.29, Rayleigh number Ra $= 10^3$–10^6, and Hartmann number for Ha = 0–120. COMSOL Multiphysics, a numerical simulation program, was used to solve the governing equations. It was demonstrated that for lower Ra values, heat transfer through an applied magnetic field is unaffected for a specific S value because the mechanism of transport is diffusion, whereas for larger Ra, there is a complex interaction among magnetic field and physical thermal properties. The features of the heat transfer rate are determined by the interaction. The Nusselt number virtually stays constant as Ha rises at smaller Ra. However, at high Ra, the Nusselt number initially declines with Ha and thereafter essentially stays constant, and at high Ra values, the switch from conduction to convective heat transfer takes place. Additionally, Nu rises slightly with S at increasing Ra.

Keywords: Nusselt number; circular enclosure; magnetic field; cylinders; natural convection

Citation: Azzouz, R.; Hamida, M.B.B. Natural Convection in a Circular Enclosure with Four Cylinders under Magnetic Field: Application to Heat Exchanger. *Processes* **2023**, *11*, 2444. https://doi.org/10.3390/pr11082444

Academic Editor: Vladimir D. Stevanovic

Received: 23 June 2023
Revised: 4 August 2023
Accepted: 11 August 2023
Published: 14 August 2023

1. Introduction

Due to its practical importance in engineering applications such heat exchangers, power systems, materials manufacturing, desalination [1,2], and thermal process protection [3,4], the buoyancy-driven convective heat transfer within enclosures has recently grown in popularity. On the one hand, the density of the fluid affects how buoyant the object is. Fluids that are denser or cooler have lower kinetic energies than fluids that are more agitated; therefore, they put less pressure on the molecules in their immediate vicinity. Compared to warmer fluids, this fluid produces less pressure, hence gravity has a greater impact on it. On the other hand, the way in which the enclosure is oriented, the form of the object within it, the different thermal limits that were employed, the heat source, and the type of convection mixed or natural convection as a mechanism have all been addressed in the majority of previous studies. A magnetic field, which causes a magnetic force and alters the flow, is one of the most important parameters in this context. This is crucial for requests in districts like the development of crystal in fluids, photoelectric bundle, and atomic reactor abating. Consequently, it is fundamental to research this top to bottom to grasp the instrument and its effect on regular convection [5–7].

The impact of articles put inside a walled-in area on heat movement has been explored broadly in light of the potential applications [8], for example, nuclear power stockpiling frameworks, warm solace in rooms, materials handling, and so on.

Two differentially heated cylinders, one of which was hot and the other cold, and which were placed in various areas of the enclosure, were the subject of research by Park et al. [9]. They also investigated the heat transfer driven by buoyancy that occurred between four hot circular cylinders that were symmetrically placed within a chilly enclosure [10]. They explained how the current stream field shifts from secure to unstable when Ra's value rises.

Roslan et al. [11] looked at how heat moved through a cylinder in a square cage with a cyclic surface temperature. In their analysis, they found that changing the cylinder's radius is what causes the greatest periodic changes in heat transfer. Cho et al. [12] investigated how heat transfer was affected by the distance in a square cage between each of the cylinders. For various cylinder geometries and wall temperatures, Bhowmick et al. [13] looked at the effect of buoyancy on the transfer of thermal energy from an enclosed heated cylinder. Other researchers calculated the heat transfer caused by buoyancy between two heated cylinders inside of an enclosure with side walls and an unevenly cooled bottom [14,15].

Pirmo et al. states that, especially at lower Ra values, the Nusselt number affects convective heat transfer in a gallium-filled enclosure which is exposed to a magnetic field [16]. Others state that, especially at low Ra values, the Nusselt number affects convective heat transfer in a gallium-filled enclosure which is exposed to a magnetic field [17].

The magnetohydrodynamic natural convection was carried out by Turkyilmazoglu [18] using a vertically stretched permeable surface heated in a porous environment using a heat source. He discovered that heat transfer depends on the heat source. Using the finite difference method, Siddiqui et al. [19] focused on the effects of cavity depth and magnetic field on flow dynamics in a porous lid-driven cavity. By altering the cavitation depth and magnetic field strength, they were able to observe distinct vortices patterns in water-based ferrofluid. Siddiqui and Turkyilmazoglu [20] explored lightness-prompted heat movement in a ferrofluid encased permeable and porous hole mounting with an attractive wire. In a rhombic Cu-water nanofluid enclosure, Dutta studied MHDNC [21].

The need for compact systems in current times has made the heat dissipation rate a matter of greater importance [22,23]. Due to their size, water cooling systems and air-cooling systems are less effective in tiny systems. In this regard, Khan N. S. et al. [24] investigates the motion of gyrotactic microorganisms and the formation of entropy by using multi-type pf nanoparticles. Also, Khan N. S. et al. [25] examined the flow of a three-dimensional Maxwell nanofluid produced by two parallel rotating disks. Additionally, this takes into account binary chemical reactions, Arrhenius activation energy, gyrotactic microorganisms with the Hall current effect, nanoparticle concentration, and heat transmission. Therefore, using nanofluids in industrial settings for heating and cooling is desirable. At the same time, cost can be reduced by enlarging the system. By increasing the rate of heat transmission, nanofluid aids in strengthening the efficiency of thermal systems. To lower the heat resistance, nanofluids are widely employed in a variety of applications, including as fuel, as an automotive coolant, in cavities [5,26,27], in electronics [28], medical equipment, as well as absorption machines and light-emitting diode (LED) [29].

Further, according to Pal et al.'s [30] investigation, diffusion is the transport method for low values of Ra, hence the applied magnetic field has no bearing on heat transfer. However, the field of magnetism and physico-thermal characteristics interact in a complex way for greater Ra, which affects how quickly heat is transferred. The time-averaged Nusselt number, at lower Ra, remains essentially unchanged with Ha. Higher Ra values, however, mark the transition between convective and conductive heat transmission, and Nut initially declines with Ha before remaining roughly constant. In addition, for higher Ra, the Nusselt number drops slightly initially due to an increase in the distance between the cylinders, then it slightly increases as the distance between cylinders increases within the square enclosure.

In addition, industrial systems are significantly more complex than a straightforward arrangement like a warm body in a frigid environment. In reality, however, there are several locations where there are many corpses enclosed. Earlier research revealed that the

number, shape, and location of hot bodies in the enclosure all have a significant impact on the transport phenomenon.

In this work, systematic studies are conducted to acquire understanding of the effects of the magnetic field (Hartman number Ha), Rayleigh number (Ra), and location of four heated cylinders on heat transmission in a circular enclosure with chilly walls.

2. Numerical Model

2.1. Simplifying Assumptions

The 2D governing equations system is solved by taking into account the following simplifying assumptions:

- The fluid used is considered incompressible and Newtonian fluid;
- The flow is thought to be stable, laminar, and two-dimensional;
- The effect of radiation considered minimal;
- Neglect is shown also for displacement currents, dissipation, and Joule heating.

Actually, the set of equations is somehow more theoretically challenging than the analogous set for totally compressible flows if the flow is assumed to be unstable and viscous, which is the same situation as for Newtonian fluid and incompressible fluid. And the use of a two-dimensional model is considered since the model being studied is symmetric and for practically the same results, it will take more time to solve it. As well as the last two assumptions, another is that mathematically, it will be complicated to resolve.

2.2. Equations of the Model

2.2.1. Dimensional Form

The balance laws of mass, linear momentum, and thermal energy in steady-state two-dimensional settings serve as the foundation for the governing equations for the issue at hand. With these presumptions in mind, the dimensional form of the simplified system of equations is as follows.

Mass conservation equation:

$$\frac{\partial u}{\partial x} + \frac{\partial v}{\partial y} = 0 \tag{1}$$

where u and v are, respectively, the velocities according to x and y.

Momentum conservation equation:

For the x-projection:

$$\left(u\frac{\partial u}{\partial x} + v\frac{\partial u}{\partial y}\right) = -\frac{1}{\rho}\frac{\partial p}{\partial x} + \frac{\mu}{\rho}\left(\frac{\partial^2 u}{\partial x^2} + \frac{\partial^2 u}{\partial y^2}\right) \tag{2}$$

where ρ and μ are, respectively, the density and the dynamic viscosity. p is the pressure.

For the y-projection:

$$\left(u\frac{\partial v}{\partial x} + v\frac{\partial v}{\partial y}\right) = -\frac{1}{\rho}\frac{\partial p}{\partial y} + \frac{\mu}{\rho}\left(\frac{\partial^2 v}{\partial x^2} + \frac{\partial^2 v}{\partial y^2}\right) + \beta g(T - T_c) - \frac{\sigma B_0^2}{\rho}v \tag{3}$$

where β represents the thermal expansion coefficient, T is the wall temperature, and T_c is the cold wall temperature. B_0 represents the strength of the magnetic field and σ is the electrical conductivity.

The energy conservation equation:

$$u\frac{\partial T}{\partial x} + v\frac{\partial T}{\partial y} = \alpha\left(\frac{\partial^2 T}{\partial x^2} + \frac{\partial^2 T}{\partial y^2}\right) \tag{4}$$

with α being the thermal diffusivity.

2.2.2. Nondimensional Form

The following defines a number of non-dimensional variables and parameters:

$$x^* = \frac{x}{L},\ y^* = \frac{y}{L},\ u^* = \frac{uL}{\alpha},\ v^* = \frac{vL}{\alpha},\ p^* = \frac{pL^2}{\rho\alpha^2},\ T^* = \frac{T - T_c}{T_h - T_c},$$
$$\mathrm{Ra} = \frac{\beta \mathrm{g} \mathrm{L}^3(\mathrm{T_h} - \mathrm{T_c})}{\upsilon\alpha},\ \mathrm{Ha} = \mathrm{B_0 L}\sqrt{\frac{\sigma}{\rho\upsilon}},\ \mathrm{Pr} = \frac{\upsilon}{\alpha},\ \alpha = \frac{\lambda}{\rho C_p},\ \mathrm{S} = \frac{s}{L},\ v = \frac{\mu}{\rho},$$

where Pr is the Prandtl number, S presents the cylinders 'distance, which has no dimensions, B_0 is the strength of the magnetic field and the thermal diffusivity α, β represents the thermal expansion coefficient, σ is the electrical conductivity, λ is the thermal conductivity, v is the kinematic viscosity, ρ is the density, and p presents the pressure, respectively. It is worth mentioning that T_h and T_c are, respectively, the hot and cold temperatures of the circulating fluid.

The governing dimensionless form of transport equations, also known as the conservation of mass, momentum, and energy, can be written as follows using these variables [23,24]:

The non-dimensional mass conservation equation:

$$\frac{\partial u^*}{\partial x^*} + \frac{\partial v^*}{\partial y^*} = 0 \tag{5}$$

The non-dimensional momentum conservation equation:

For the x-projection:

$$\frac{1}{\mathrm{Pr}}\left[u^*\frac{\partial u^*}{\partial x^*} + v^*\frac{\partial u^*}{\partial y^*}\right] = -\frac{1}{\mathrm{Pr}}\frac{\partial p^*}{\partial x^*} + \left(\frac{\partial^2 u^*}{\partial x^{*2}} + \frac{\partial^2 u^*}{\partial y^{*2}}\right) \tag{6}$$

For the y-projection:

$$\left(u\frac{\partial v}{\partial x} + v\frac{\partial v}{\partial y}\right) = -\frac{1}{\rho}\frac{\partial p}{\partial y} + \frac{\mu}{\rho}\left(\frac{\partial^2 v}{\partial x^2} + \frac{\partial^2 v}{\partial y^2}\right) + \beta g(T - T_c) - \frac{\sigma B_0^2}{\rho}v \tag{7}$$

$$\frac{L^3}{v\alpha} \times \left[\left(u\frac{\partial v}{\partial x} + v\frac{\partial v}{\partial y}\right) = -\frac{1}{\rho}\frac{\partial p}{\partial y} + \frac{\mu}{\rho}\left(\frac{\partial^2 v}{\partial x^2} + \frac{\partial^2 v}{\partial y^2}\right) + \beta g(T - T_c) - \frac{\sigma B_0^2}{\rho}v\right] \tag{8}$$

$$\frac{L}{v} \times \left[\frac{\frac{L}{\alpha}}{\frac{1}{L}} \times u\frac{\partial v}{\partial x} + \frac{\frac{L}{\alpha}}{\frac{1}{L}} \times v\frac{\partial v}{\partial y}\right]$$
$$= -\frac{\alpha}{\nu} \times \frac{L^1}{\rho\alpha^2} \times L\frac{\partial p}{\partial y} + \left(\frac{\frac{L}{\alpha}}{\frac{1}{L^2}} \times \frac{\partial^2 v}{\partial x^2} + \frac{\frac{L}{\alpha}}{\frac{1}{L^2}} \times \frac{\partial^2 v}{\partial y^2}\right) \tag{9}$$
$$+ \frac{L^3}{v\alpha} \times \beta g(T - T_c) \times \frac{T_h - T_c}{T_h - T_c} - \frac{L^3}{v\alpha} \times \frac{\sigma B_0^2}{\rho}v$$

$$\frac{\alpha}{\nu}\left[\frac{uL}{\alpha} \times \frac{\partial\left(\frac{vL}{\alpha}\right)}{\partial\left(\frac{x}{L}\right)} + \frac{vL}{\alpha} \times \frac{\partial\left(\frac{vL}{\alpha}\right)}{\partial\left(\frac{y}{L}\right)}\right]$$
$$= -\frac{\alpha}{v} \times \frac{\partial\left(\frac{pL^2}{\rho\alpha^2}\right)}{\partial\left(\frac{y}{L}\right)} + \left(\frac{\partial^2\left(\frac{vL}{\alpha}\right)}{\partial\left(\frac{x}{L}\right)^2} + \frac{\partial^2\left(\frac{vL}{\alpha}\right)}{\partial\left(\frac{y}{L}\right)^2}\right) \tag{10}$$
$$+ \frac{\beta g L^3(T_h - T_c)}{v\alpha} \times \frac{T - T_c}{T_h - T_c} - B_0^2 L^2 \frac{\sigma}{\rho v} \times \frac{vL}{\alpha}$$

$$\frac{1}{\mathrm{Pr}}\left[u^*\frac{\partial v^*}{\partial x^*}+v^*\frac{\partial v^*}{\partial y^*}\right]=-\frac{1}{\mathrm{Pr}}\frac{\partial p^*}{\partial y^*}+\left(\frac{\partial^2 v^*}{\partial x^{*2}}+\frac{\partial^2 v^*}{\partial y^{*2}}\right)+\mathrm{Ra}T^*-Ha^2v^* \tag{11}$$

The non-dimensional energy conservation equation:

$$u^*\frac{\partial T^*}{\partial x^*}+v^*\frac{\partial T^*}{\partial y^*}=\frac{1}{\mathrm{Pr}}\left(\frac{\partial^2 T^*}{\partial x^{*2}}+\frac{\partial^2 T^*}{\partial y^{*2}}\right) \tag{12}$$

2.2.3. Boundary Conditions

Figure 1a depicts the physical model and coordinate system. A water-filled circular enclosure of length L makes up the computational domain. Along the horizontal mid-plane, four cylinders with a diameter of d (or $0.2 \times L$) are positioned at a specific distance s apart. Laminar, two-layered, and incompressible fluid flow is considered present. The Boussinesq approximation yields constant fluid properties (Pr = 6.58). Viscous dissipation and radiative heat transfer effects are not taken into account. The outer wall of the nook is maintained at temperature Tc and the inner chambers are kept up with at a T_h temperature ($>T_c$).

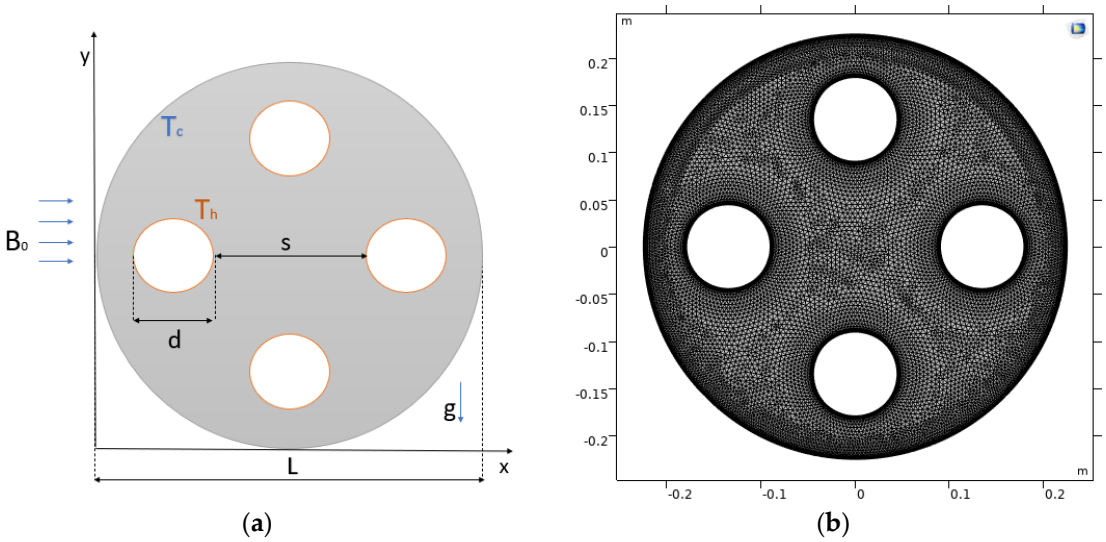

(**a**) (**b**)

Figure 1. (**a**) Physical model; (**b**) meshed domain for S = 0.2.

On the cylinders surfaces and the outer big cylinder's wall, we establish boundary requirements for the velocity that are free of slip and penetration. For the four cylinders, the surface temperatures of the heated cylinders are the same and uniform. In addition, the temperature of the outer big cylinder is the same throughout.

The limit conditions on the chamber surfaces are:

$$u^*=v^*=0;\ T^*=1 \tag{13}$$

At the enclosure's walls:

$$u^*=v^*=0;\ T^*=0 \tag{14}$$

We start with zero magnetic vector potential in all directions and atmospheric pressure throughout the domain.

By doing the study listed below on the temperature gradient in the normal direction, each location on the cylinder surface may have its local Nusselt number determined:

$$\mathrm{Nu}=-\left.\frac{\partial \mathrm{T}^*}{\partial \eta}\right|_{\text{cylinder surface}} \tag{15}$$

η is a normal-direction dimensionless coordinate here.

The governing Equations (1)–(12) are solved using the computer program COMSOL Multiphysics (version 6.1) with the mandated boundary conditions.

The computational domain is initially divided into elements and subdomains. The meshed processing area for S = 0.2 is shown in Figure 1b. The interface of the software uses the finite element approach to solve the partial differential governing equations of transport. This solver makes use of two distinct modules to tackle both heat transfer and flow simultaneously. The "heat transfer" module is employed to assess the thermal field, whereas the "laminar flow" module is employed to assess the velocity field.

3. Results and Discussion

3.1. Validation

By contrasting the results with those of G.C. Pal et al. [30] for $20 \leq Ha \leq 120$, Ra between 10^3 and 10^6, the correctness of the proposed calculations was verified in a square enclosure filled with ethylene glycol-Cu nanofluids for heated circular coils within a cold enclosure under a magnetic field. With a solid capacity percentage of 0.05, the mean Nusselt number for different Hartmann numbers (Ha), is compared with the results of G.C. Pal et al. [30] in Table 1.

Table 1. Validation in numerical code at $Ra = 10^5$ and $Ra = 10^6$.

Ha	Nu Present Work At $Ra=10^5$	G.C. Pal et al. [30] At $Ra = 10^5$	Nu Present Work At $Ra=10^6$	G.C. Pal et al. [30] At $Ra = 10^6$
20	1.3467	1.44	3.0546	3.00
40	1.2980	1.20	2.4429	2.50
60	1.1330	1.10	2.1916	2.22
80	1.0487	0.98	1.8428	1.77
100	1.0039	0.96	1.7782	1.70
120	0.9777	0.96	1.5753	1.47

We analyze buoyant heat transfer using four hot embedded cylinders embedded in a circular enclosure exposed to a magnetic field that is applied from outside.

In this study, the Rayleigh number is between 10^3 and 10^6; the Hartmann number is bounded by 0 and 120. As well, the dimensionless distance ranges are $0.05 \leq S \leq 0.29$.

3.2. Flow Field

We start by looking at streamlines in terms of how Ha, Ra, and S interact to affect the flow features. In Figures 2 and 3, respectively, only the results for $Ra = 10^5$ and 10^6 are displayed due to space restrictions.

It is noticeable that the fluid near the heated four cylinders heats up and flows to the ends of the big cylinder. However, after coming into touch with the nearby cool surface, the fluid particles drop, creating recirculation zones. As shown in Figure 2, the vortices appear to intensify evenly toward the cylinder's extreme walls at $Ra = 10^5$. This is a result of the convection influence, which is more prevalent at significantly greater Ra and eventually boosts the power of those vortices. Since the buoyant force is suppressed by the magnetic force, it is evident that increasing Ha causes the vortices' intensity to diminish. Four essentially symmetrical recirculating cells form atop the cylinders with lower Ha values for $Ra = 10^5$ and 10^6. When the value of Ha rises above 60, these cells produce a variety of recirculating cells that surround the heated cylinders.

For a variety of S, the effect of Ha is shown in Figures 2 and 3. As can be seen at $S = 0.05$, the top wall of the cylinder is surrounded by only four recirculating cells that are symmetrical along the vertical axis for $Ha = 20$. As Ha rises, these cells gradually move farther from the center of the cylinders. However, with $S = 0.2$ toward the cylinder's

top surface, the variety of recirculating cells rises to seven. The recirculating cells become longer and encroach into the cylinder spaces as the S levels rise further.

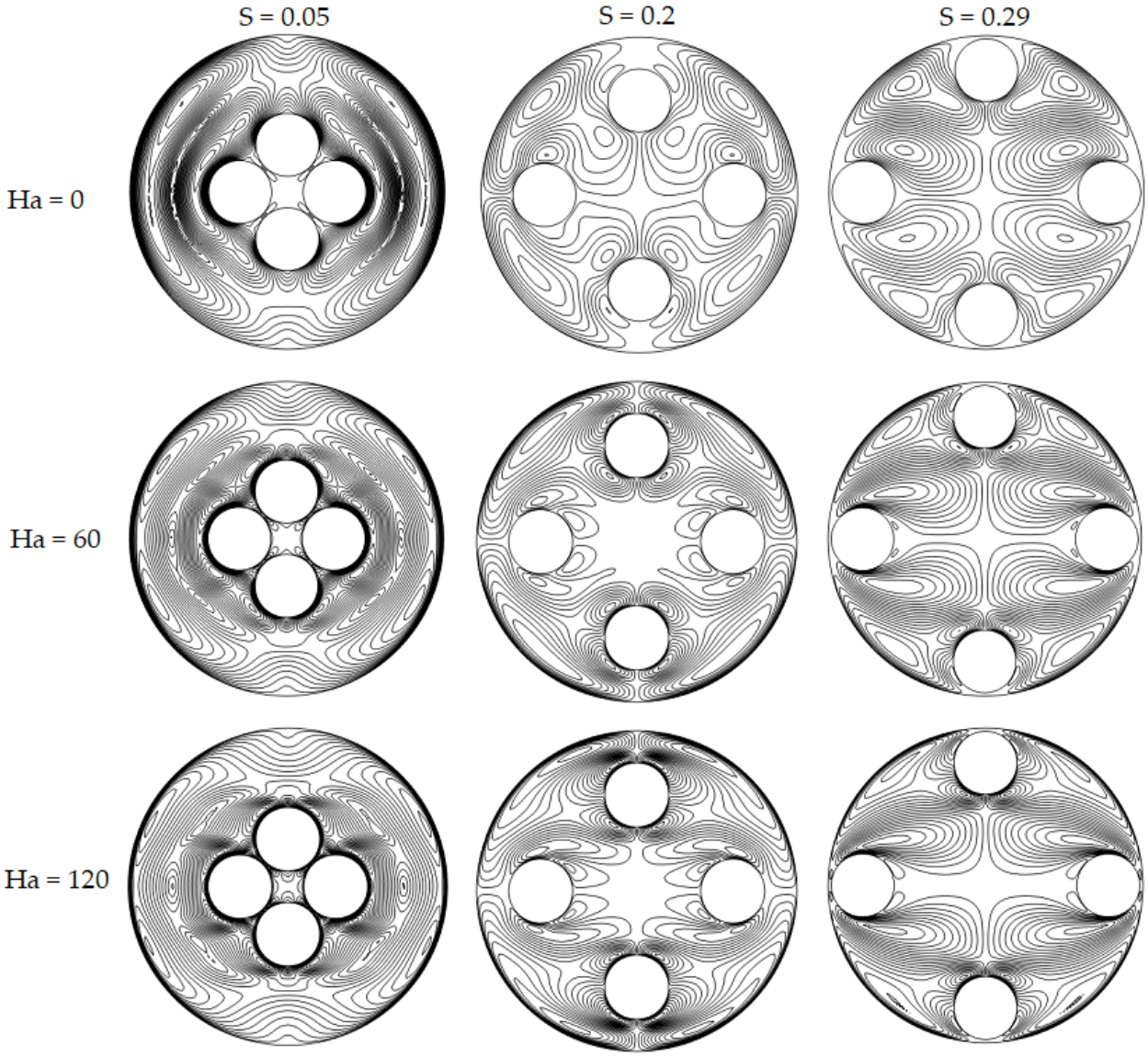

Figure 2. Streamlines at Ra $= 10^5$ at various values of Ha and S.

At larger values of Ha, it is discovered that the streamline pattern is symmetric along both the vertical and horizontal axes. By increasing S, symmetry was attained at Ha ≥ 60. The recirculation areas grow as S increases because there is less wall friction and more room for the fluid to circulate between the cylinders.

Additionally, it is crucial to remember that the convective impact effect, which causes the heated fluid to climb toward the cylinder's wall and cause the development of recirculating zones in the enclosure, cannot be suppressed by the magnetic field at lower values of Ha.

An intriguing phenomenon in the streamline distribution is seen as Ha increases. The fluid moves toward the enclosure's center as the convective flow is partially suppressed. This finally results in the growth of recirculating cells that are symmetrical both vertically and horizontally. The magnetic force, even at its highest strength, has no impact on the flow pattern at Ra $= 10^6$, even if the streamline pattern continues to have the same spacing as described at Ra $= 10^5$. This is because the buoyancy force is so strong.

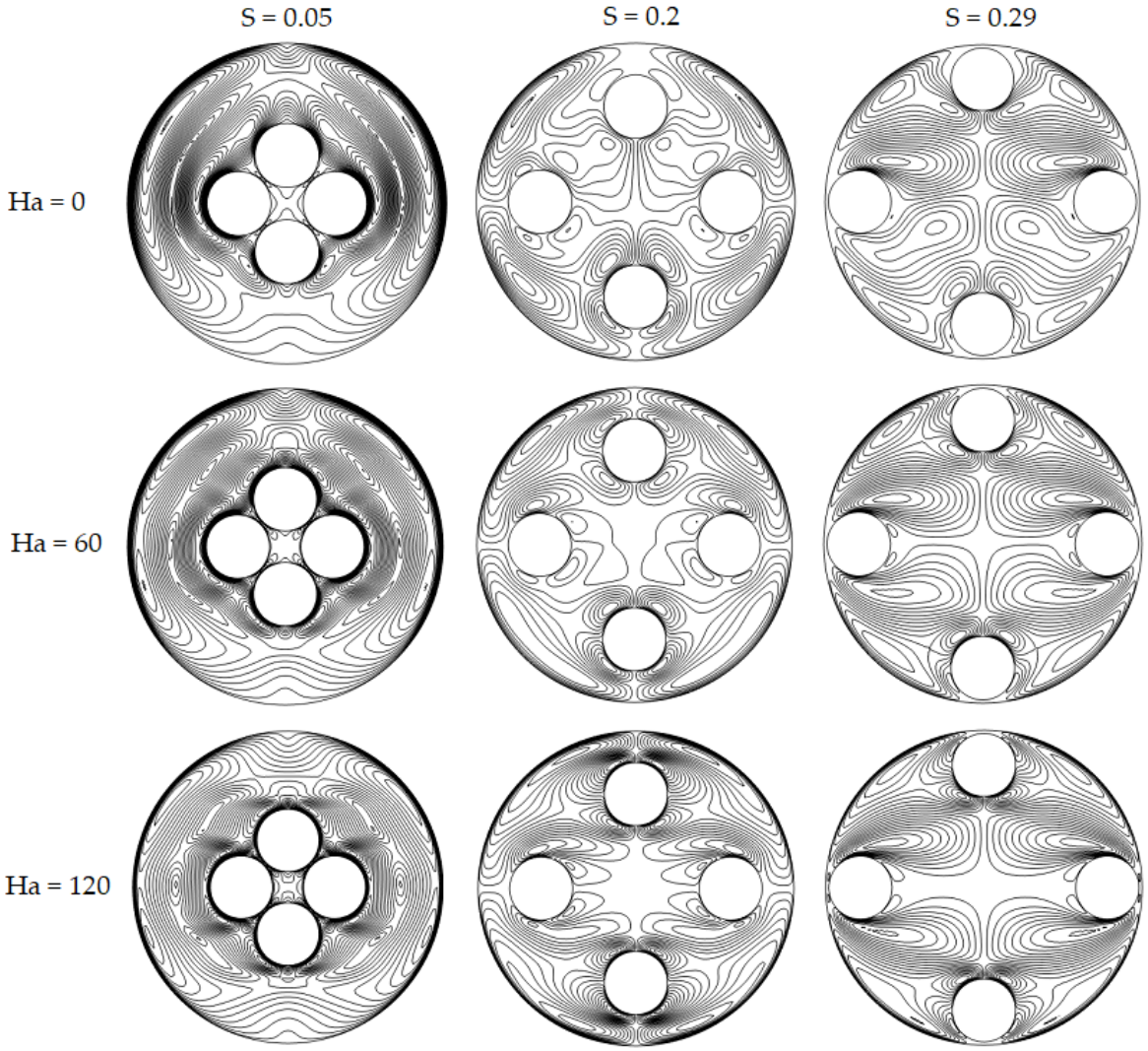

Figure 3. Streamlines at Ra $= 10^6$ at various values of Ha and S.

Additionally, the majority of the recirculation cells are formed around the enclosure's external walls.

3.3. Temperature Field

Figure 4 depicts a detailed investigation of the isotherms that are useful for understanding the physics involved in heat transmission.

Particularly for Ra $\leq 10^4$, isotherms are evenly spaced and approximately parallel to one another, and the values they have are extremely significant in the area around the cylinders no matter how close the cylinders are to other objects or how far away they are from other objects or from other objects, regardless of Ha, demonstrating that conduction is the main mechanism for heat transfer.

The isotherms around the cylinders travel higher for S = 0.05 when Ra approaches 10^5, showing the strength of the buoyant force. Additionally, isotherms between the cylinders migrate upward for S = 0.2 and S = 0.29, demonstrating the supremacy of the buoyant force.

As the magnetic field's (Ha) intensity rises, the convective flow weakens. Therefore, when Ra grows, the isotherms typically position themselves in a parallel pattern independent of the spacing S. When Ra $= 10^6$, and convection flow reaches its highest point with an elevated advection rate, a plume of temperature forms that pushes the fluid towards the upper edge of the cylindrical enclosure. Because of this, the isotherms are deformed close to the exterior wall of the cylinders, but Regardless of S and Ha, they remain parallel underneath the cylinders.

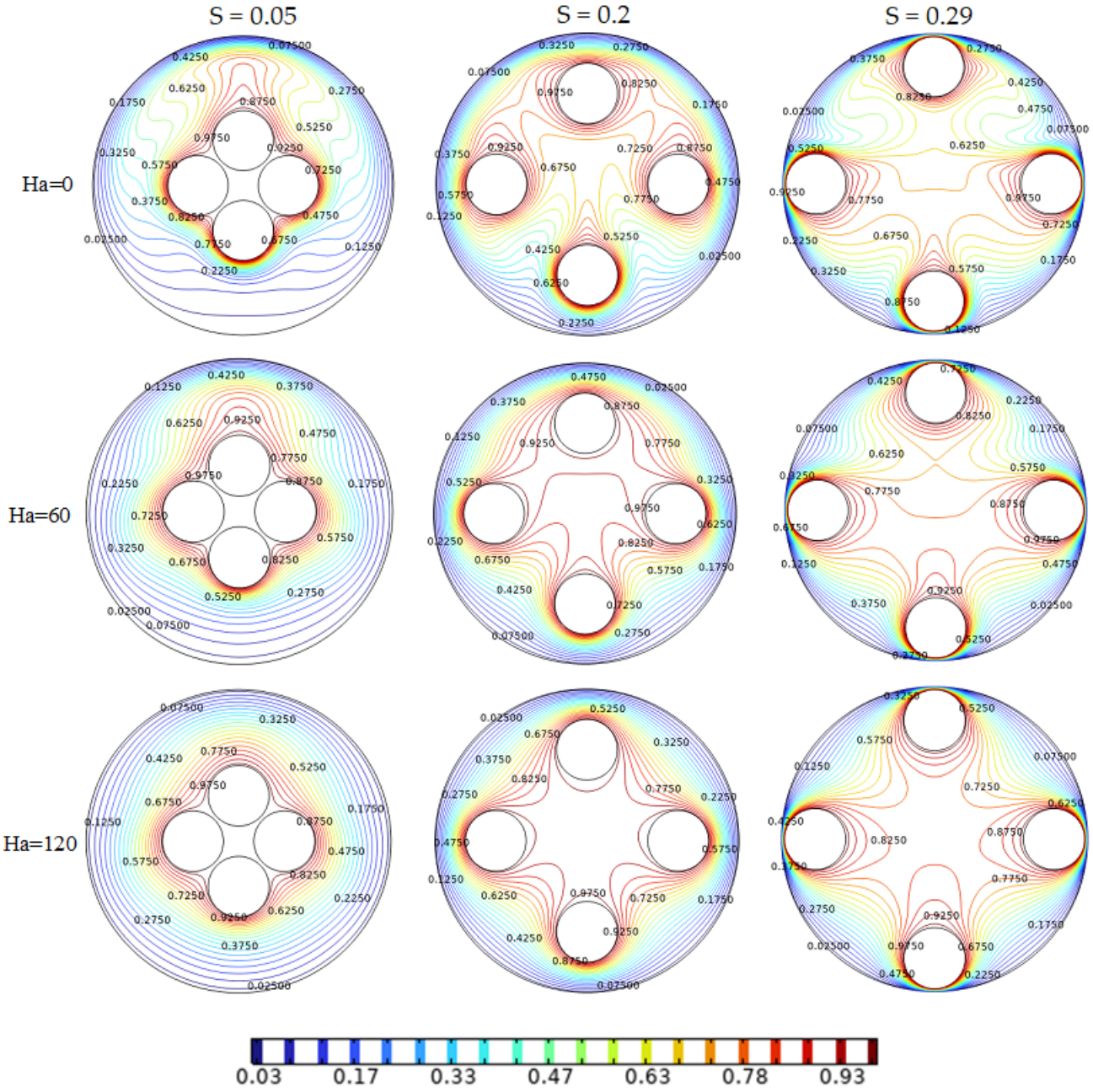

Figure 4. Isotherms at Ra $= 10^6$ at various values of Ha and S.

However, with Ha, the isotherms towards the top edge of the cylinders are less distorted. The motion of the fluid seeping into the gap between the cylinders and the orthogonally produced magnetic force, which decreases buoyancy, are the main contributors to this. This penetration rises with S, as can be observed. Also noteworthy is the close proximity of the isotherms at Ha 60 to the heated cylinders with Ra, which are equal to 10^5 and 10^6.

At Ha > 60, the magnetic field controls the convection flow, causing the isotherms to be less closely packed together near the cylinders. Regardless of Ha, the isotherms are tightly packed within the huge cylinder's side wall and its hot inner areas for S = 0.29 and Ra $= 10^5$ and 10^6.

3.4. Heat Transfer

The effect of Ha out of Nu for different S and Ra values is shown in Figure 5. As the diffusion of the rate of heat transfer predominates at reduced values of Ra (Ra $\leq 10^4$), and

for a given S value, Nu is virtually constant and is barely influenced by Ha. The magnetic force rises in strength at Ra = 10^5, preventing buoyant forces induced by the rate of heat transfer, although Nu decreases constantly with Ha up to about Ra = 60. Considering the exception that with slightly larger Ha values Nu almost becomes constant, between Ha = 100 and 120, whereas Nu is significantly greater at Ra = 10^5, this exhibits comparable tendencies for 10^6 value of Ra. The thermal characteristics of the space between heated cylinders are significantly influenced by the regime of Ra and Ha.

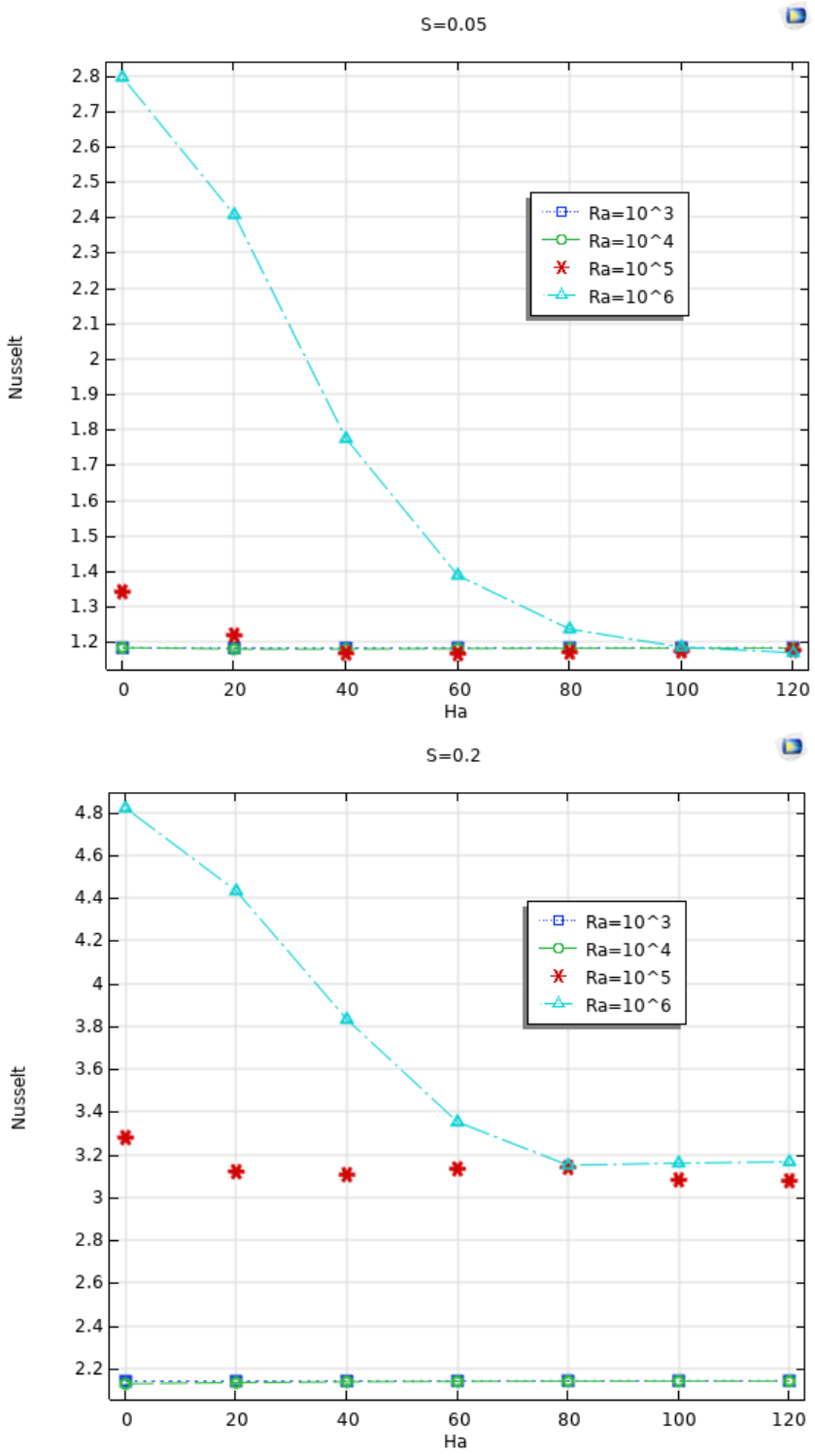

Figure 5. *Cont.*

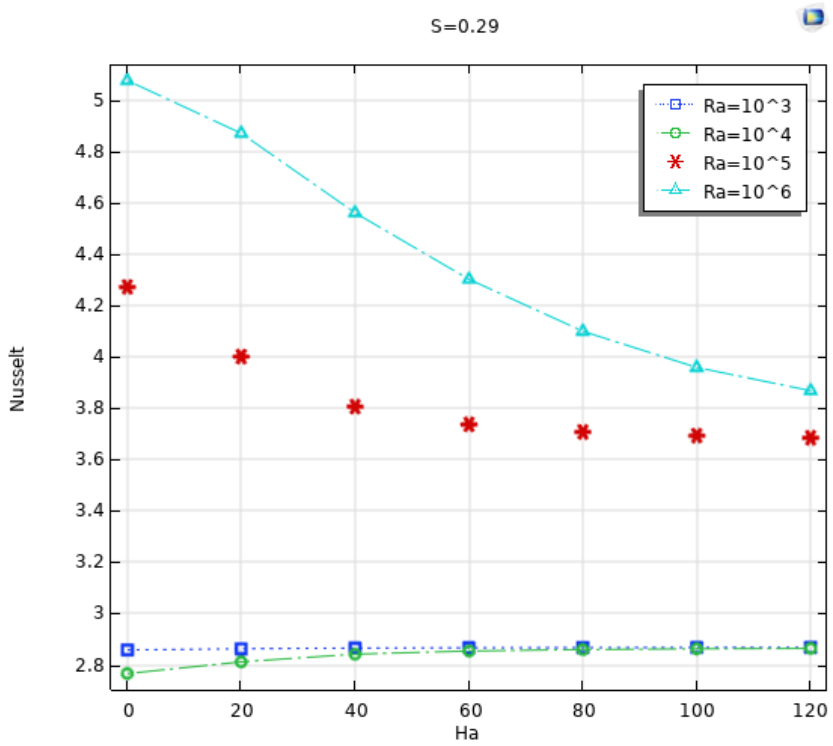

Figure 5. Nu variation with Ha at various values of Ra and S.

For any Ra values in the selected region, Nu grows with S during the application of an outside magnetic field of a particular value. A possible reason is that the temperature gradient on the cylinder surfaces is higher on the entire surface for larger S values than it is for smaller S values. A greater Nusselt number is produced by a small increase in the temperature gradient at higher S values.

When the magnetic field present is equal to zero (Ha = 0), Nu rises with S. In the case of S = 0.05, 0.2, and 0.29, respectively, the values of Nu are 1.34, 3.27, and 4.27 for Ra = 10^5 and Ha = 0. Also, the equivalent numbers are 2.84, 4.89, and 5.14 for Ra = 10^6 at Ha = 0.

The creation of plumes and fluid deluge are examples of other elements that affect the transport characteristics, even though the effects of S on the features of heat transport are the same as when there are situations with smaller amounts of Ra. Furthermore, the inter-spacing distance has a significant impact on how thermal plumes surrounding the cylinder merge.

4. Conclusions

For the dimensionless distance S = 0.05–0.29 between all inner cylinders, the number assigned by Rayleigh is Ra = 10^3–10^6 and the Hartmann number is Ha = 0–120. In the current work, buoyancy-driven heat transfer among four warmed cylinders inside a cold cylindrical enclosure is investigated numerically in two dimensions.

The fluid is Newtonian and incompressible. The following is a summary of the major findings:

Four symmetrical recirculating zones (around the vertical midline) and lower values of Ra are discovered to be independent of S and Ha. (10^4). For Ra = 10^5 and 10^6, four symmetrical recirculating cells surround the heated cylinders for lower Ha values. When the value of Ha approaches 60, these cells expand to the right and left sides of the heated cylinders and create a variety of recirculating cells beyond the vertical mid-plane.

Regardless of Ha, the isotherms remain parallel and have very high data close to the cylinders at lower values of Ra (10^4). When Ra hits 10^5, the isotherms between the cylinders start to move, and regardless of the spacing S, as Ha rises, the potential for the isotherms to align parallelly grows. The isotherms become distorted close to the top of the cylinders

when Ra $= 10^6$, but they remain nearly parallel to one another in the region under the cylinders regardless of Ha as well as S. This occurs as a result of the fluid being pushed toward the top surface of the cage by a thermal plume that is generated.

The Nusselt number (Nu) for lower Ra is essentially unchanged by Ha. Higher Ra values mark the change from conductive to convective heat transmission, with Nu initially decreasing with Ha and subsequently remaining about constant.

So, as a conclusion of this work, now that we have checked the outer results after changing the inner spacing between the four inner cylinders, we can say that the second case with S = 0.2 is the most significant one compared to the others.

Author Contributions: Conceptualization, M.B.B.H.; methodology, M.B.B.H.; software, M.B.B.H.; validation, M.B.B.H.; formal analysis, R.A. and M.B.B.H.; investigation, R.A. and M.B.B.H.; resources, R.A.; data curation, R.A.; writing—original draft preparation, R.A. and M.B.B.H.; writing—review and editing, R.A. and M.B.B.H.; visualization, R.A. and M.B.B.H.; supervision, M.B.B.H. All authors have read and agreed to the published version of the manuscript.

Funding: This research received no external funding.

Institutional Review Board Statement: Not applicable.

Informed Consent Statement: Not applicable.

Data Availability Statement: The data presented in this study are available on request from the corresponding author.

Acknowledgments: The authors would like to acknowledge the support provided by the Research Laboratory of Ionized backgrounds and Reagents Studies (EMIR) at the Preparatory Institute for Engineering Studies of Monastir (IPEIM)-Tunisia. The investigation presented in this paper was conducted as part of the research thesis in Physics Engineering at the Higher School of Sciences and Technology of Hammam Sousse (ESSTHS)-Tunisia supervised By Mohamed Bechir Ben Hamida.

Conflicts of Interest: The authors declare no conflict of interest.

Nomenclature

B_0	Magnetic field strength
g	Gravitational acceleration, (ms^{-2})
Ha	Hartmann number
L	Length of cavity, (m)
Nu	Nusselt number
p	Fluid pressure, $Pa = Nm^{-2}$
p^*	Dimensionless pressure
Pr	Prandtl number
Ra	Rayleigh number
T	Temperature, (K)
T^*	Dimensionless temperature
s	Distance between inner cylinders (m)
S	Dimensionless distance between cylinders
d	Diameter of inner cylinder
T_h	Temperature of hot fluid, (K)
T_c	Temperature of cold fluid, (K)
MHDNC	magnetohydrodynamic natural convection
u, v,	Velocity components in x, and y directions
u^*, v^*,	Dimensionless velocity components
x, y,	Cartesian coordinates
x^*, y^*,	Dimensionless coordinates
α	Thermal diffusivity, m^2s^{-1}
λ	Thermal conductivity, $Wm^{-1}K^{-1}$
Cp	Specific heat capacity, $JKg^{-1}K^{-1}$
σ	Electrical conductivity, AmV^{-1}
β	Expansion coefficient, K^{-1}

ρ	Density, kg m^{-3}
υ	Cinematic viscosity, $m^2 s^{-1}$
η	Normal direction dimensionless coordinate
c	Cold
h	Hot

References

1. Ben Hamida, M.B. Numerical analysis of tubular solar still with rectangular and cylindrical troughs for water production under vacuum. *J. Taibah Univ. Sci.* **2023**, *7*, 2159172. [CrossRef]
2. Ben Hamida, M.B.; Al Shammari, F.; Altawi, I.; Alhadri, M.; Almeshaal, M.A.; Hajlaoui, K. Potential of tubular solar still with rectangular trough for water production under vacuum condition. *Therm. Sci.* **2022**, *26*, 4271–4283.
3. Ben Hamida, M.B.; Belghaieb, J.; Hajji, N. Nnumerical study of heat and mass transfer enhancement for bubble absorption process ofammonia-water mixture without and with nanofluids. *Therm. Sci.* **2018**, *22*, 3107–3120.
4. Tayebi, T.; Dogonchi, A.S.; Chamkha, A.J.; Ben Hamida, M.B.; El-Sapa, S.; Galal, A.M. Micropolar nanofluid thermal free convection and entropy generation through an inclined I-shaped enclosure with two hot cylinders. *Case Stud. Therm. Eng.* **2022**, *31*, 101813. [CrossRef]
5. Massoudi, M.D.; Ben Hamida, M.B.; Mohammed, H.A.; Almeshaal, M.A. MHD Heat Transfer in W-Shaped Inclined Cavity Containing a Porous Medium Saturated with Ag/Al_2O_3 Hybrid Nanofluid in the Presence of Uniform Heat Generation/Absorption. *Energies* **2020**, *13*, 3457. [CrossRef]
6. Massoudi, M.D.; Ben Hamida, M.B.; Almeshaal, M.A.; Hajlaoui, K. The influence of multiple fins arrangement cases on heat sink efficiency of MHD MWCNT-water nanofluid within tilted T-shaped cavity packed with trapezoidal fins considering thermal emission impact. *Int. Commun. Heat Mass. Transf.sf.* **2021**, *126*, 105468. [CrossRef]
7. Ben Hamida, M.B.; Charrada, K. Natural convection heat transfer in an enclosure filled with an ethylene glycol—Copper nanofluid under magnetic fields. *Numer. Heat Transf. A-Appl.* **2015**, *67*, 902–920. [CrossRef]
8. Baranwal, A.K.; Chhabra, R.P. Effect of fluid yield stress on natural convection from horizontal cylinders in a square enclosure. *Heat Tran. Eng.* **2017**, *38*, 557–577. [CrossRef]
9. Park, Y.G.; Yoon, H.S.; Ha, M.Y. Natural convection in square enclosure with hot and cold cylinders at different vertical locations. *Int. J. Heat Mass. Transf.* **2012**, *55*, 7911–7925. [CrossRef]
10. Park, Y.G.; Ha, M.Y.; Yoon, H.S. Study on natural convection in a cold square enclosure with a pair of hot horizontal cylinders positioned at different vertical locations. *Int. J. Heat Mass Transf.* **2013**, *65*, 696–712. [CrossRef]
11. Roslan, R.; Saleh, H.; Hashim, I.; Bataineh, A.S. Natural convection in an enclosure containing a sinusoidally heated cylindrical source. *Int. J. Heat Mass Transf.* **2014**, *70*, 119–127. [CrossRef]
12. Cho, H.W.; Seo, Y.M.; Mun, G.S.; Ha, M.Y.; Park, Y.G. The effect of instability flow for two-dimensional natural convection in a square enclosure with different arrays of two inner cylinders. *Int. J. Heat Mass Transf.* **2017**, *114*, 307–317. [CrossRef]
13. Bhowmick, D.; Randive, P.; Pati, S.; Agrawal, H.; Kumar, A.; Srivastava, P.K. Natural convection heat transfer and entropy generation from a heated cylinder of different geometry in an enclosure with non-uniform temperature distribution on the walls. *J. Therm. Anal. Calorim.* **2020**, *141*, 839–857. [CrossRef]
14. Deka, D.K.; Pal, G.C.; Pati, S.; Randive, P.R. Natural convection from two cylinders in an enclosure with sinusoidal bottom wall: A numerical study. In *Recent Advances in Mechanical Engineering*; Lecture Notes in Mechanical Engineering; Springer: Singapore, 2021; pp. 351–359.
15. Goswami, N.; Randive, P.R.; Pati, S. Natural convection from a pair of heated cylinders in a square cavity with non-uniform temperature on the side walls. *J. Inst. Eng.* **2021**, *102*, 389–396. [CrossRef]
16. Pirmohammadi, M.; Ghassemi, M. Effect of magnetic field on convection heat transfer inside a tilted square enclosure. *Int. Commun. Heat Mass. Transf.* **2009**, *36*, 776–780. [CrossRef]
17. Ghasemi, B.; Aminossadati, S.M.; Raisi, A. Magnetic field effect on natural convection in a nanofluid-filled square enclosure. *Int. J. Therm. Sci.* **2011**, *50*, 1748–1756. [CrossRef]
18. Turkyilmazoglu, M. MHD natural convection in saturated porous media with heat generation/absorption and thermal radiation: Closed-form solutions. *Arch. Mech.* **2019**, *71*, 49–64.
19. Siddiqui, A.A.; Turkyilmazoglu, M. A new theoretical approach of wall transpiration in the cavity flow of the ferrofluids. *Micromachines* **2019**, *10*, 373. [CrossRef]
20. Siddiqui, A.A.; Turkyilmazoglu, M. Natural convection in the ferrofluid enclosed in a porous and permeable cavity. *Int. Commun. Heat Mass. Transf.* **2020**, *113*, 104499. [CrossRef]
21. Dutta, S.; Goswami, N.; Biswas, A.K.; Pati, S. Numerical investigation of magnetohydrodynamic natural convection heat transfer and entropy generation in a rhombic enclosure filled with Cu-water nanofluid. *Int. J. Heat Mass. Transf.* **2019**, *136*, 777–798. [CrossRef]
22. Ben Hamida, M.B.; Almeshaal, M.A.; Hajlaoui, K. A Three-dimensional thermal analysis for cooling a square Light Emitting Diode by Multiwalled Carbon Nanotube-nanofluid-filled in a rectangular microchannel. *Adv. Mech. Eng.* **2021**, *13*, 16878140211059946. [CrossRef]

23. Ben Hamida, M.B.; Hatami, M. Investigation of heated fins geometries on the heat transfer of a channel filled by hybrid nanofluids under the electric field. *Case Stud. Therm. Eng.* **2021**, *28*, 101450. [CrossRef]
24. Khan, N.S.; Poom, K.; Thounthong, P. Mechanical aspects of Maxwell nanofluid in dynamic system with irreversible analysis. *Int. J. Heat Mass Transf.* **2019**, *145*, 118713. [CrossRef]
25. Khan, N.S.; Shah, Q.; Sohail, A.; Poom, K. Renewable energy technology for the sustainable development of thermal system with en-tropy measures. *ZAMM-J. Appl. Math. Mech./Z. Für Angew. Math. Und Mech.* **2021**, *101*, e202000212.
26. Kefayati, G.H.R. Lattice Boltzmann simulation of MHD natural convection in a nanofluid-filled cavity with sinusoidal temperature distribution. *Powder Technol.* **2013**, *243*, 171–183. [CrossRef]
27. Al-Zamily, A.; Meerali, J. Effect of magnetic field on natural convection in a nanofluid-filled semi-circular enclosure with heat flux source. *Comput. Fluids* **2014**, *103*, 71–85. [CrossRef]
28. Aglawe, K.R.; Yadav, R.K.; Thool, S.B. Preparation, applications and challenges of nanofluids in electronic cooling: A systematic review. *Mater. Today Proc.* **2021**, *43*, 366–372. [CrossRef]
29. Ben Hamida, M.B.; Hatami, M. Optimization of fins arrangements for the square light emitting diode (LED) cooling through nanofluid-filled microchannel. *Sci. Rep.* **2021**, *11*, 12610. [CrossRef] [PubMed]
30. Pal, G.C.; Nammi, G.; Pati, S.; Randive, P.R.; Baranyi, L. Natural convection in an enclosure with a pair of cylinders under magnetic field. *Case Stud. Therm. Eng.* **2022**, *30*, 101763. [CrossRef]